Supporting Information

Text S1 Biochar preparation and characterization

After pyrolysis of carp residues in muffle furnace, the biochars were ground and filtered by a 0.17 mm sieve, then stored for characterization analysis and adsorption experiments. To prepare the demineralized biochars (DRCBs), the pristine biochars were washed in constant temperature oscillator (150 r/min, 25℃) with 0.1 mol/L HCl. Subsequently, the DRCBs were washed with pure water when the pH of the leaching solution kept unchanging. Studies from Cui et al. (2016) have showed that the acid leaching process did not change the oxygen-containing functional groups (OFGs) on biochar. Then, the DRCBs were dried at 75℃ for 12 h, then ground and filtered by a 0.17 mm sieve. Finally, these DCRBs were labeled as DCRB450, DCRB550, and DCRB650, respectively.

The zeta potentials of CRBs were determined by a Zetasizer (SZ-100, Japan). The pH of all CRBs were obtained by adding CRBs (1 mg) to deionized water (pH 7.0, 10 mL) and shaking for 1 h at 150 r/min (Zhao et al., 2022). The specific surface area and porisity of CRBs were detected using micromeritics (ASAP2020C, USA). Total of the CRBs were determined by an elemental analyzer (Micro Cube, Elementar, Germany). Thermal analysis of CRBs was measured by STA 449 (NETZSCH, Germany). The morphology and elemental composition (C, H, N, and O) of biochars were analyzed by using JSM-7800F scanning electron microscopy (SEM) coupled with electron dispersive X-ray analysis (EDX) and thermogravimetric analyzer (STA449F5, Netzsch, Germany). The surface functional groups were detected by X-ray diffraction and X-ray photoelectron spectroscopy (XPS, ESCALAB 250Xi, USA) and Fourier transform infrared spectroscopy (FTIR) (Bruker, TENSOR 27, Germany).

Text S2 The adsorption kinetics and isotherms of Cu on CRBs

The adsorption kinetics process of Cu^{2+} adsorption on biochars were fitted by using the pseudo-first-order equation (Eq. (S1)), the pseudo-second-order equation (Eq. (S2)), the Elovich equation (Eq. (S3)) and the intra-particle diffusion equation (Eq. (S4)), and the equations were as follows (Tran et al., 2017; Deng et al., 2019):

$$dQ_t/dt = k_1 (Q_e - Q_t) \quad , \qquad \text{(S1)}$$

$$dQ_t/dt = k_2 (Q_e - Q_t)^2 \quad , \qquad \text{(S2)}$$

$$Q_t = (\ln(ab) + \ln t)/b \quad , \qquad \text{(S3)}$$

$$Q_t = k_d t^{1/2} + a_i \quad , \qquad \text{(S4)}$$

where Q_t (mg/g) and Q_e (mg/g) are the corresponding adsorptive quantities at time t and adsorption equilibrium, respectively. K_1 (min) and k_2 (g/mg/min) are the rate constant of the pseudo-first-order equation and the pseudo-second-order equation, respectively. K_d (mg/g/min$^{1/2}$) is the apparent diffusion rate constants. a (mg/g/min) and b (g/mg) are the initial adsorption rate constant and a parameter of the Elovich equation, respectively. B is related to the extent of surface coverage and activation energy for chemisorption. a_i (mg/g) is a constant representing the thickness of the liquid film.

The isothermal adsorption process of Cu^{2+} adsorption on CRBs were fitted to the Langmuir model (Eq. (S5)), the Freundlich model (Eq. (S6)), the Sips model (Eq. (S7)) and the Temkin model (Eq. (S8)), and the equations were as follows (Tran et al., 2017; Deng et al., 2019):

$$Q_e = Q_m K_L C_e/(1 + K_L C_e) \quad , \qquad \text{(S5)}$$

$$Q_e = K_F C_e^{1/n} \quad , \qquad \text{(S6)}$$

$$Q_e = Q_m K_S C_e^{1/n} (1 + K_S C_e^{1/n}) \quad , \qquad \text{(S7)}$$

$$Q_e = A\ln K_T C_e \quad , \qquad \text{(S8)}$$

where C_e (mg/L) is the Cu^{2+} concentration. Q_e (mg/g) is the sorption capacity of Cu^{2+} at equilibrium. Q_m (mg/g) is the saturated sorption capacity for monolayer adsorption. K_L (L/mg), K_F (mg/g), K_S (L$^{1/n}$/mg$^{1/n}$) and K_T (L/mg) are the adsorption coefficient of the Langmuir, the Freundlich, Sips, and Temkin model. The n represents the dimensionless constant, which indicates the adsorption intensity. A (kJ/mol) is the coefficient associated to the heat of adsorption.

The adsorption efficiency of adsorbents can be analyzed by the separation factor (R_L). The calculation equation is as follows (Zhao et al., 2010):

$$R_L = 1/(1 + K_L C_0) \quad , \qquad \text{(S9)}$$

where K_L is the angmuir constant. C_0 is the initial Cu^{2+} concentration. $0 < R_L < 1$ indicates that the adsorption process is favorable, $1 < R_L$ indicates that the adsorption process is unfavorable, $R_L = 1$ indicates that the adsorption process is linear, and $R_L = 0$ indicates that the adsorption process is irreversible.

Table S1 Pyrolytic temperature selected to prepare different biowaste-derived biochars in literature.

Adsorbents	Temperature (℃)	References
silvergrass, *Enteromorpha prolifera*, and seaweed residue-derived biochar	300, 500, 700	Zhao et al., 2022
Pig carcass-derived biochar	650	Yang et al., 2022
Wheat straw biochar	300, 450, 600	Yin et al., 2017
Fish bone-based biochar	550, 700, 900	Módenes et al., 2020
Fish-scale biochar	450, 600, 750	Xia et al., 2022
Carp residues-derived biochar	450, 550, 650	This study

Table S2 Intra-particle diffusion model parameters for Cu^{2+} sorption on CRBs.

Sample[α)]	a_1[β)] (mg/g)	k_{d1} (mg/g/min$^{1/2}$)	R^2	a_2 (mg/g)	k_{d2} (mg/g/min$^{1/2}$)	R^2
CRB450	1.308	3.939	0.9375	17.37	0.639	0.9924
CRB550	4.599	7.345	0.9931	32.72	1.639	0.9876
CRB650	7.648	6.843	0.9955	29.86	2.541	0.9896

Notes: α) CRB450, CRB550 and CRB650 were the carp residue-derived biochars produced at 450℃, 550℃ and 650℃, respectively. β) a_i: the thickness of the liquid film, mg/g. k_{di}: the rate constant of apparent diffusion rate constants, in the intra-particle diffusion equation, mg/g/min$^{1/2}$.

Table S3 Summary of the literature data on adsorption of Cu^{2+} on different adsorbents.

Adsorbents	T_p α) (℃)	t_p β) (h)	Conditions of adsorption experiments					Q_m δ) (mg/g)	References
			adsorbent dose (g/L)	C_0 γ) (mg/L)	pH	T (℃)	t (h)		
Chitosan saturated montmorillonite	NA ε)	NA ε)	0.4	2–96	5.0	25	24	34.91	Hu et al., 2017
Cellulose nanofibrils	NA ε)	NA ε)	1	1–300	NA ε)	30	24	52.32	Zhang et al., 2016
Acai Brazil nut Palm kernel cake	700	1	0.2	0–224	4.5	25	24	5 6 6.5	Dias et al., 2019
Modified cellulose	NA ε)	NA ε)	0.5	0–50	4.0	25	48	6.86	Huang et al., 2018
Date-palm waste biomass biochar	800	NA ε)	1	50–250	5.5	30	0.5	52.08	Amin et al., 2019
Wheat straw biochar	300 450 600	1	5	20–500	6.0	25	72	28.60 38.70 44.30	Yin et al., 2017
Date seed biochar	550	3	10	19–254	6.0	25	24	26.75	Mahdi et al., 2018
Cattle biochar Swine biochar Cattle manure biochar Swine manure biochar Poultry manure biochar	500	4	5	0–635.5	NA ε)	25	24	66.72 74.35 49.57 44.48 43.21	Lei et al., 2019
Carp residues-derived biochar	450 550 650	6	1	20–150	5.5	25	5	26.95 58.82 62.50	This study

Notes: α) T_p: the pyrolytic temperature in the preparation of biochar, ℃. β) t_p: the pyrolytic time, h. γ) C_0: the initial concentration of Cu^{2+} in the adsorption process, mg/L. δ) Q_m: the maximum adsorption capacity of Cu^{2+} on biochars obtained by Langmuir model, mg/g. ε) NA: indicates that the data is not obtained.

Table S4 The atomic ratio (%) of the main elements in SEM-EDS elemental dot maps.

Element	Atomic (%)					
	CRB450α)	Cu-loaded CRB450	CRB550α)	Cu-loaded CRB550	CRB650α)	Cu-loaded CRB650
C	79.60	37.47	35.07	75.66	28.19	62.92
O	8.43	45.93	42.78	10.72	43.69	26.71
P	0.68	6.09	6.54	1.49	9.36	3.83
Ca	0.14	7.39	13.32	1.09	16.34	4.59
Cu	0	2.77	0	0.31	0	0.74

Notes: α) CRB450, CRB550 and CRB650 were the carp residue-derived biochars produced at 450℃, 550℃ and 650℃, respectively.

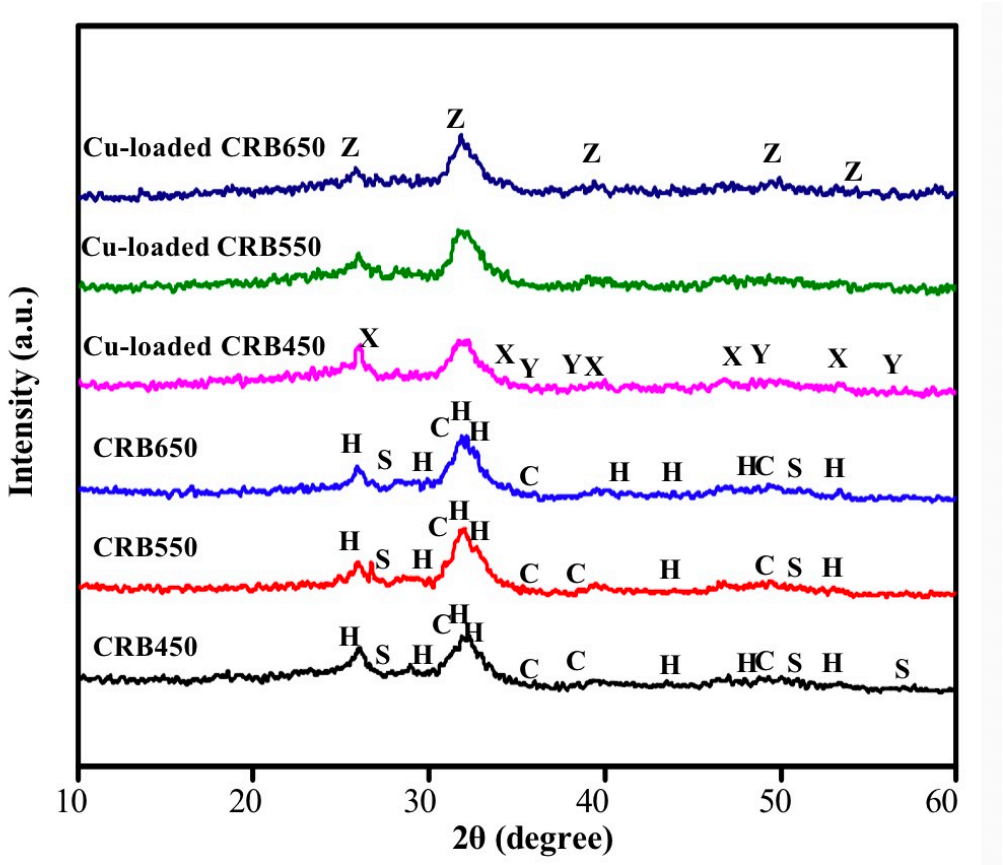

Fig. S1 XRD patterns of biochars prepared at different temperatures before and after adsorption of Cu. CRB450, CRB550 and CRB650 were the carp residue-derived biochars produced at 450℃, 550℃ and 650℃, respectively. The letters in the figure represent characteristic peaks corresponding to different substances, C represents the $CaCO_3$, S represents the KCl, X corresponds to the cupric hydroxide, Y corresponds to the cupric oxide, and Z represents the Cu-phosphate precipitation. H contains the following substances: hydroxyapatite (HAP), $Ca_5(PO_4)_3X$, $Ca_{10}(PO_4)_6X_2$, X=Cl^-, or OH^-.

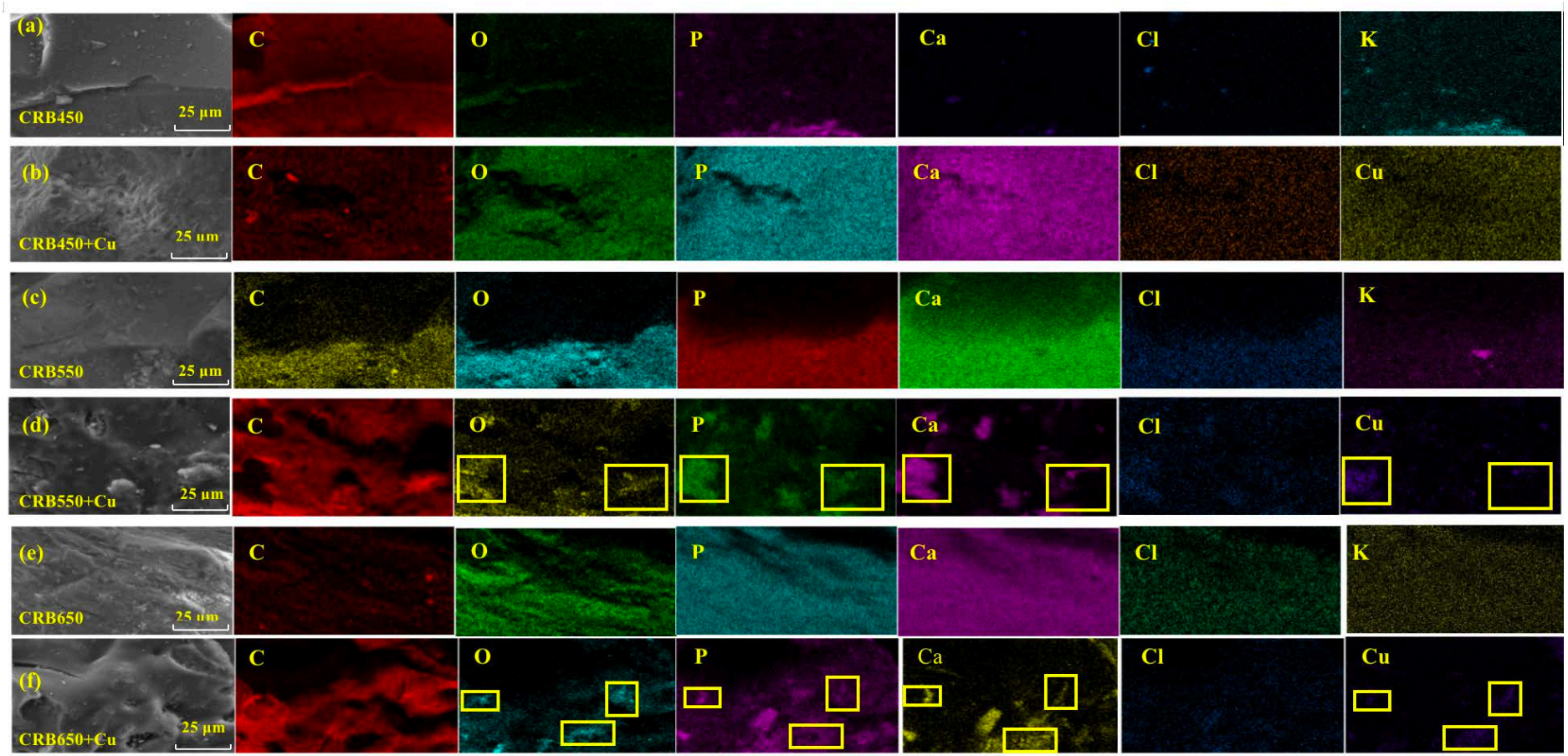

Fig. S2 SEM images and elemental dot maps of CRB450 (a, b), CRB550 (c, d), and CRB650 (e, f) before and after Cu^{2+} adsorption. The elemental mapping of CRBs in the panel: C, O, P, Ca, Cl, and K (a, c, e), while the elemental mapping of CRBs after Cu^{2+} adsorption in the panel: C, O, P, Ca, Cl, and Cu (b, d, f). The yellow rectangle indicated that the Cu adsorption was related to the relevant functional groups or the release of cations and anions, such as the exchange of Cu^{2+} and Ca^{2+} on CRBs. CRB450, CRB550 and CRB650 were the carp residue-derived biochars produced at 450℃, 550℃ and 650℃, respectively.

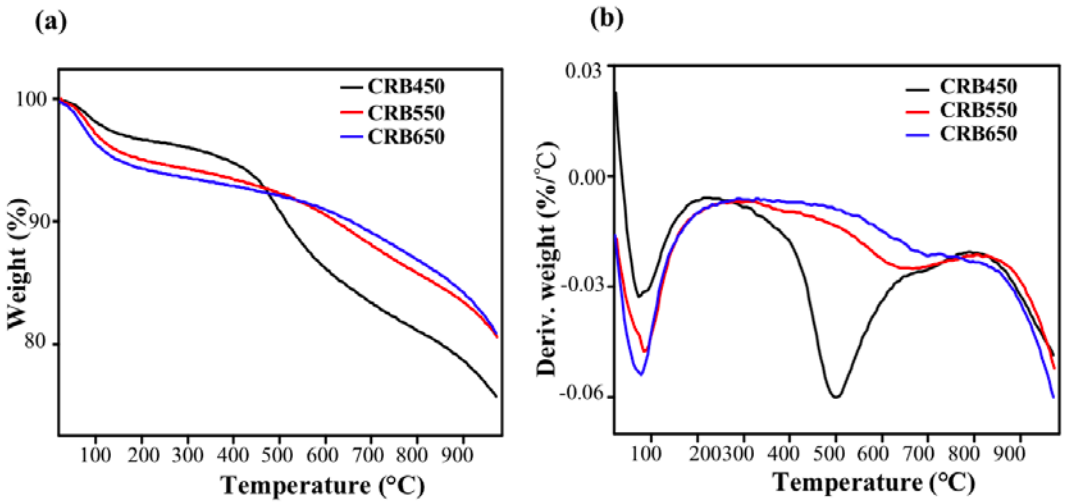

Fig. S3 Thermogravimetric analysis (TGA) (a) and differential thermal gravimetric curves (b) of CRBs derived at 450℃–650℃. CRB450, CRB550 and CRB650 were the carp residue-derived biochars produced at 450℃, 550℃ and 650℃, respectively.

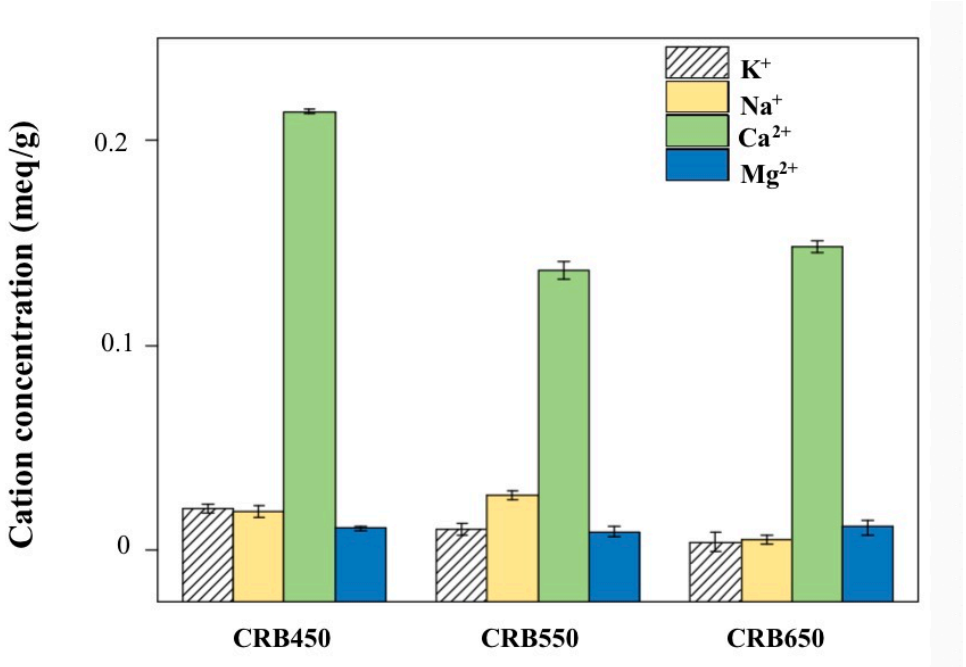

Fig. S4 The content of released cations (K^+, Ca^{2+}, Na^+, and Mg^{2+}) from CRBs. CRB450, CRB550 and CRB650 were the carp residue-derived biochars produced at 450℃, 550℃ and 650℃, respectively. The error bars represent standard deviation (n =3).

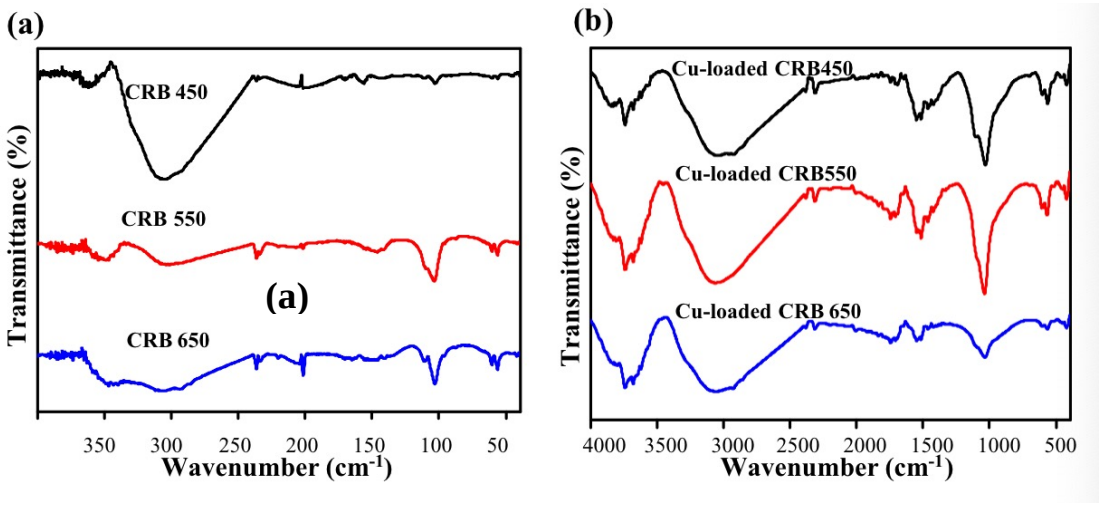

Fig. S5 FTIR spectra of CRBs (a) and Cu-loaded CRBs (b). The bands at 2013, 1029, 563 and 468 cm^{-1} were attributed to the v_1, v_3, v_4 and v_2 modes of PO_4^{3-} (Markovic et al., 2004; Lei et al., 2019), respectively. The bands at 1458 and 875 cm^{-1} were attributed to the v_3 and v_2 modes of CO_3^{2-} (Lei et al., 2019), respectively. In addition, biochars also contained more organic functional groups, including phenolic-OH (3498 cm^{-1}), CO-OH (3034 cm^{-1}), C-H bonds in aromatic group (2916 cm^{-1}), C≡C (2200 cm^{-1}), N-H (2362 cm^{-1}), C=C (1649 cm^{-1}), C-O-C (1103 cm^{-1}), and C=O (1560 cm^{-1}) (Lei et al., 2019).

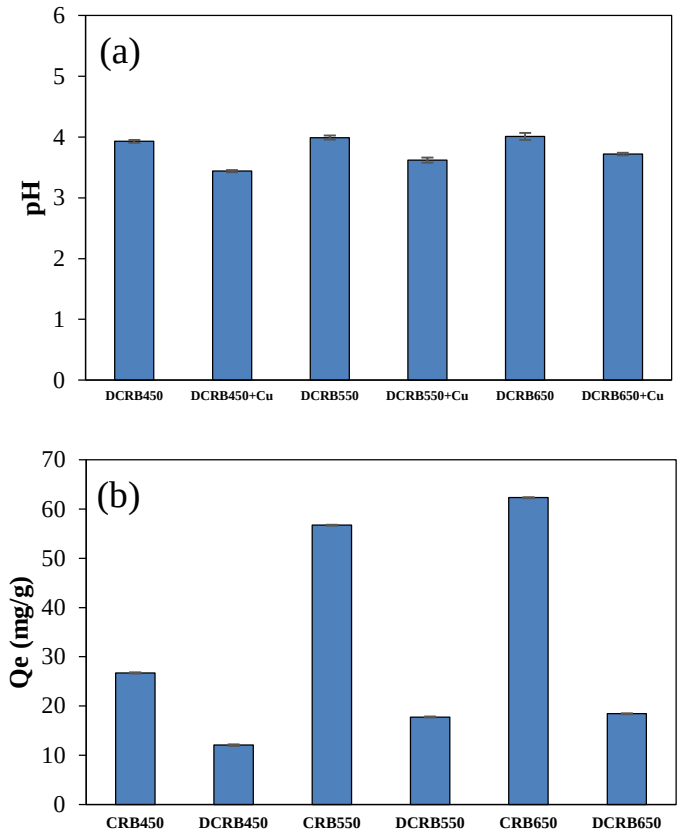

Fig. S6 The pH change of the mixed solution of demineralized biochars with and without Cu^{2+} after equilibration with the initial pH of all solution was 5.0 (a). The adsorption capacity of Cu^{2+} on the pristine biochars (CRBs) and demineralized biochars (DCRBs) (b). CRB450, CRB550 and CRB650 were the carp residue-derived biochars produced at 450℃, 550℃ and 650℃ respectively. The error bars represent standard deviation (n =3).

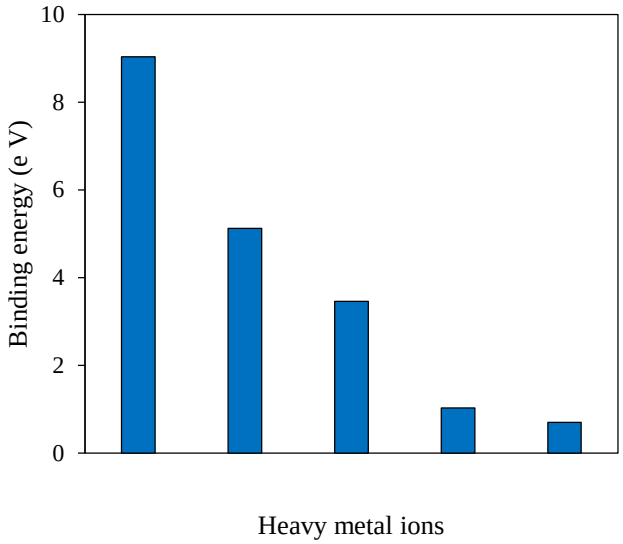

Fig. S7 The binding energy between the heavy metal ions (K^+, Na^+, Ca^{2+}, Mg^{2+} and Cu^{2+}) and the benzene ring (electron-rich π-systems) through the G09 package.

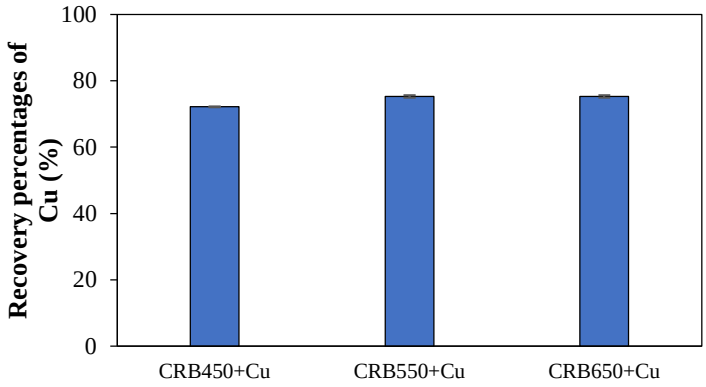

Fig. S8 The sequential extraction recovery percentages of Cu^{2+} from Cu-loaded biochars. CRB450, CRB550 and CRB650 were the carp residue-derived biochars produced at 450℃, 550℃ and 650℃, respectively. The error bars represent standard deviation (*n* =3).

References

Amin M T, Alazba A A, Shafiq M (2019). Application of biochar derived from date palm biomass for removal of lead and copper ions in a batch reactor: kinetics and isotherm scrutiny. Chemical Physics Letters, 722(1): 64–73

Cui X, Fang S, Yao Y, Li T, Ni Q, Yang X, He Z (2016). Potential mechanisms of cadmium removal from aqueous solution by Canna indica derived biochar. Science of the Total Environment, 562(15): 517–525

Deng Y, Huang S, Larid D A, Wang X, Meng Z (2019). Adsorption behaviour and mechanisms of cadmium and nickel on rice straw biochars in single- and binary-metal systems. Chemosphere, 218: 308–318

Dias Y N, Souza E S, Costa H S C, Melo L C A, Penido E S, Amarante C B, Teixeira O M M, Fernandes A R (2019). Biochar produced from Amazonian agro-industrial wastes, properties and adsorbent potential of Cd2+ and Cu2+. Biochar, 1(4): 389–400

Hu C, Zhu P, Hu H, Fu Q (2017). Comparative adsorption of Pb (II), Cu (II) and Cd (II) on chitosan saturated montmorillonite: kinetic, thermodynamic and equilibrium studies. Applied Clay Science, 143: 320–326

Huang Z, Huang Z, Feng L, Luo X, Wu P, Cui L, Mao X (2018). Modified cellulose by polyethyleneimine and ethylenediamine with induced Cu (II) and Pb (II) adsorption potentialities. Carbohydrate Polymers, 202(15): 470–478

Lei S, Shi Y, Qiu Y, Che L, Xue C (2019). Performance and mechanisms of emerging animal-derived biochars for immobilization of heavy metals. Science of the Total Environment, 646(1): 1281–1289

Mahdi Z, Yu Q J, Hanandeh A E (2018). Investigation of the kinetics and mechanisms of nickel and copper ions adsorption from aqueous solutions by date seed derived biochar. Journal of Environmental Chemical Engineering, 6(1): 1171–1181

Markovic M, Fowler B O, Tung M S (2004). Preparation and comprehensive characterization of a calcium hydroxyapatite reference material. Journal of Research of the National Institute of Standards and Technology, 109(6): 553–568

Módenes A N, Bazarin G, Borba C E, Locatelli P, Scheufele F B (2020). Tetracycline adsorption by tilapia fish bone-based biochar: mass transfer assessment and fixed-bed data prediction by hybrid statistical-phenomenological modeling. Journal of Cleaner Production, 279: 123775

Tran H N, You S J, Hosseini-Bandegharaei A, Chao H P (2017). Mistakes and inconsistencies regarding adsorption of contaminants from aqueous solutions: a critical review. Water Research, 120(1): 88–116

Xia D, Liu Y, Cheng X, Gu P, Chen Q, Zhang Z (2022). Temperature-tuned fish-scale biochar with two-dimensional homogeneous porous structure: a promising uranium extractant. Applied Surface Science, 591: 153136

Yang X, Hinzmann M, Pan H, Wang J, Bolan N, Tsang D C, Rinklebe J (2022). Pig carcass-derived biochar caused contradictory effects on arsenic mobilization in a contaminated paddy soil under fluctuating controlled redox conditions. Journal of Hazardous Materials, 421(5): 126647

Yin Y, Zhu S, Xu D, Chu L, Chen C, Zhao J, Shang J (2017). Comparison of copper adsorption onto wheat biochar and ethanol-modified biochar. Nongye Huanjing Kexue Xuebao, 36(9): 1877–1883 (in Chinese)

Zhang N, Zang G, Shi C, Yu H, Sheng G (2016). A novel adsorbent TEMPO-mediated oxidized cellulose nanofibrils modified with PEI: preparation, characterization, and application for Cu (II) removal. Journal of Hazardous Materials, 316(5): 11–18

Zhao M, Ma X, Liao X, Cheng S, Liu Q, Wang H, Zheng H, Li X, Luo X, Zhao J, Li F, Xing B (2022). Characteristics of algae-derived biochars and their sorption and remediation performance for sulfamethoxazole in marine environment. Chemical Engineering Journal, 430(4): 133092

Zhao Y, Zhang B, Zhang X, Wang J, Liu J, Chen R (2010). Preparation of highly ordered cubic NaA zeolite from halloysite mineral for adsorption of ammonium ions. Journal of Hazardous Materials, 178(1–3): 658–664